AD-A074 803 NAVAL RESEARCH LAB WASHINGTON DC F/G 20/7
EQUILIBRIUM AND PROPAGATION OF A ROTATING RELATIVISTIC ELECTRON--ETC(U)
SEP 79 J D SETHIAN, K A GERBER, D N SPECTOR
UNCLASSIFIED NRL-MR-4071 NL

| OF |
AD A074 803

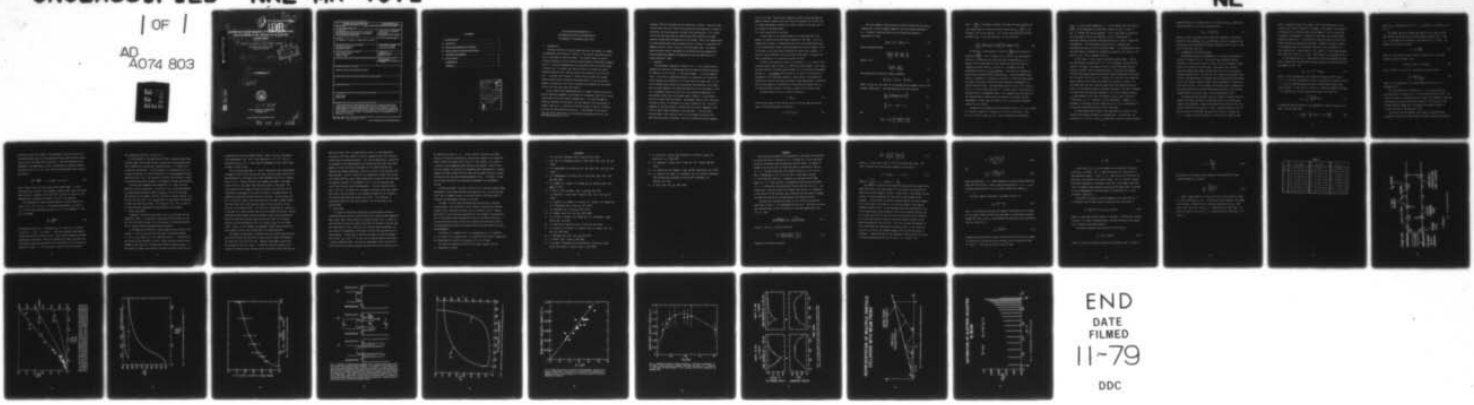

END
DATE FILMED
11-79
DDC

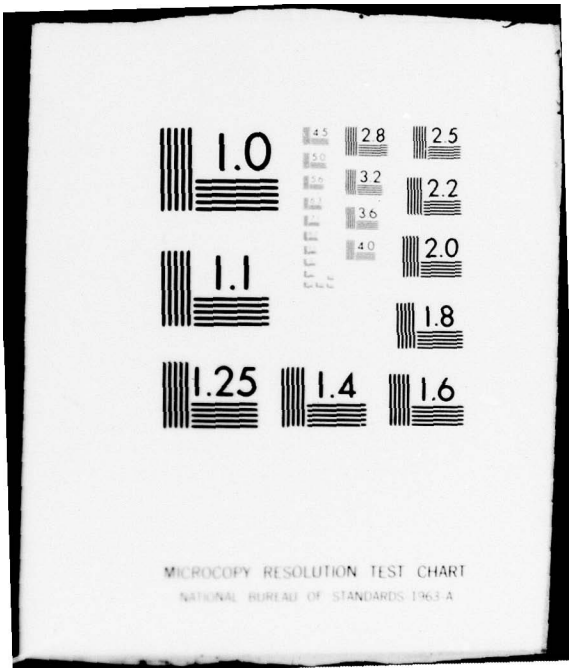
1.0
1.1
1.25
1.4
1.6
2.8
3.2
3.6
4.0
2.5
2.2
2.0
1.8
MICROCOPY RESOLUTION TEST CHART
NATIONAL BUREAU OF STANDARDS 1963-A

NRL-MR-

NRL Memorandum Report 4071

LEVEL II

Equilibrium and Propagation of a Rotating Relativistic Electron Beam in the Absence of an External Guide Field

J. D. SETHIAN, K. A. GERBER, D. N. SPECTOR AND A. E. ROBSON

Experimental Plasma Physics Branch
Plasma Physics Division

Interim rept.

28 Sept[illegible] 1979

36

NAVAL RESEARCH LABORATORY
Washington, D.C.

SECURITY CLASSIFICATION OF THIS PAGE (When Data Entered)

REPORT DOCUMENTATION PAGE		READ INSTRUCTIONS BEFORE COMPLETING FORM
1. REPORT NUMBER NRL Memorandum Report 4071	2. GOVT ACCESSION NO.	3. RECIPIENT'S CATALOG NUMBER
4. TITLE (and Subtitle) EQUILIBRIUM AND PROPAGATION OF A ROTATING RELATIVISTIC ELECTRON BEAM IN THE ABSENCE OF AN EXTERNAL GUIDE FIELD		5. TYPE OF REPORT & PERIOD COVERED Interim report on a continuing NRL problem. 6. PERFORMING ORG. REPORT NUMBER
7. AUTHOR(s) J. D. Sethian, K. A. Gerber, D. N. Spector and A. E. Robson		8. CONTRACT OR GRANT NUMBER(s)
9. PERFORMING ORGANIZATION NAME AND ADDRESS Naval Research Laboratory Washington, DC 20375		10. PROGRAM ELEMENT, PROJECT, TASK AREA & WORK UNIT NUMBERS NRL Problem 67H02-28B
11. CONTROLLING OFFICE NAME AND ADDRESS Office of Naval Research Arlington, Virginia		12. REPORT DATE September 28, 1979 13. NUMBER OF PAGES 35
14. MONITORING AGENCY NAME & ADDRESS(if different from Controlling Office)		15. SECURITY CLASS. (of this report) UNCLASSIFIED 15a. DECLASSIFICATION/DOWNGRADING SCHEDULE

16. DISTRIBUTION STATEMENT (of this Report)

Approved for public release; distribution unlimited.

17. DISTRIBUTION STATEMENT (of the abstract entered in Block 20, if different from Report)

18. SUPPLEMENTARY NOTES

19. KEY WORDS (Continue on reverse side if necessary and identify by block number)

Electron beams
Rotating beams

20. ABSTRACT (Continue on reverse side if necessary and identify by block number)

This paper describes an experimental and theoretical study of a charge-neutralized, hollow, rotating relativistic electron beam propagating inside a metal tube in the absence of an external magnetic guide field. A model has been developed in which the radial equilibrium is derived from the force balance on the beam interacting with its self-field, and the velocity of propagation of the beam is derived from the power balance. The experimental results show close agreement with the predictions of the model.

DD FORM 1 JAN 73 1473 EDITION OF 1 NOV 65 IS OBSOLETE
S/N 0102-014-6601

SECURITY CLASSIFICATION OF THIS PAGE (When Data Entered)

CONTENTS

I. INTRODUCTION 1

II. APPARATUS 2

III. RADIAL EQUILIBRIUM OF THE BEAM 3

IV. PROPAGATION OF THE ROTATING BEAM 7

V. FURTHER EXPERIMENTS 11

VI. CONCLUSIONS 13

REFERENCES 15

APPENDIX 17

EQUILIBRIUM AND PROPAGATION OF A ROTATING RELATIVISTIC ELECTRON BEAM IN THE ABSENCE OF AN EXTERNAL GUIDE FIELD

I. Introduction

Rotating relativistic electron beams have been the subject of a number of experimental and theoretical studies,[1-9] principally concerned with the use of such beams for heating plasmas. The rotating beams are usually created by passing a hollow cylindrical beam through a non-adiabatic magnetic cusp,[10,11] and are propagated down an axial guide field into either plasma or neutral gas. In neutral gas, the self-field of the beam can readily exceed the applied field, and thus reverse the direction of the field on axis. In plasma, field reversal is more difficult because the induced plasma currents tend to neutralize the beam current; it can be achieved, however, by making the rise time of the beam long compared with the transit time of an Alfven wave across the radius.[12]

It has recently been demonstrated that an intense rotating relativistic electron beam can propagate in the absence of an external guide field, inside a metal tube filled with neutral hydrogen gas.[13] The rotating beam was formed by creating a hollow beam in an axial magnetic field and passing it through a 'half-cusp', in which the field was brought to zero in a distance less than the beam electron gyro-radius. In the absence of the applied field the radial equilibrium of the beam was determined by the axial and

Note: Manuscript submitted July 5, 1979.

azimuthal fields of the beam and the induced wall currents. Since the total flux was zero, the axial fields inside and outside the beam were in opposite directions, and thus produced a reversed field configuration. This configuration was then maintained for some 18 μsec after formation by plasma currents induced when the beam had left the system. Thus it was demonstrated that the rotating beam could be used to set up a plasma in a reversed field geometry inside a closed, initially field-free metal tube. The present paper describes further experiments on the generation and propagation of rotating beams and compares the observations with the predictions of a simple theoretical model.

II. Apparatus

The experimental apparatus is shown in Fig. 1. The rotating beam is produced by injecting an annular beam from the modified TRITON accelerator ($V \gtrsim 900$ kV, $I \lesssim 80 - 110$ kA, $\tau \gtrsim 100$ nsec) through a half-cusp magnetic field. This field is generated by means of a solenoidal coil around the carbon cathode, which contains a 15 cm long ferrite cylinder, and a 1.3 cm thick aluminum plate placed 0.2 cm beyond the aluminized Mylar foil anode, which excludes magnetic flux during the 400 μsec rise of the magnetic field. This arrangement ensures that the field lines emanate perpendicular to the cathode surface, but are diverted radially outward in the shortest possible distance from the cathode. Measurements show the axial field goes from 90% to 10% of its strength in an axial distance of 2 cm. The axial component of the beam velocity interacts with the radial component of the field to impart angular momentum to the electrons.[15] The resulting rotating beam is then injected into a 14.6 cm diameter stainless steel tube containing neutral hydrogen. There is no externally-applied magnetic

field in the tube. The principal diagnostics used to study the beam are magnetic probes to measure both axial (B_z) and azimuthal (B_θ) fields, end-on framing photographs to measure the radial position of the beam, and X-ray studies of the beam density.

III. Radial equilibrium of the beam

A simple model of the rotating beam will be developed here, with emphasis on explaining the macroscopic behavior of the beam. It will be assumed that the beam is charge-neutralized, but not current-neutralized, so that electrostatic effects can be neglected and the self magnetic field of the beam is not significantly modified by plasma return currents. In practice, these conditions can be satisfied if the beam is injected into neutral hydrogen at fill pressures of about 150 mTorr.

Consider a hollow beam of radius r_b, thickness $\delta \ll r_b$, inside a flux-conserving metal tube of radius r_w in which the total magnetic flux is zero. The beam contains N electrons per cm length, all of which have an azimuthal velocity v_θ. The <u>average</u> axial velocity is v_b, which is the velocity of propagation of the beam head, however a later section is anticipated by pointing out that the individual electrons in the beam may move in both the positive and negative z-directions with velocities much greater than v_b. For the preliminary analysis, the beam is taken to be infinitely long.

The beam current (in c.g.s. units) is given by:

$$I = Nev_b \ , \tag{1}$$

and the pitch angle of this current (which is not the same as the pitch angle of the beam electrons) is given by:

$$\alpha = \tan^{-1}(v_\theta / v_b) \ . \tag{2}$$

The axial magnetic fields inside and outside the beam are B_{zi} and B_{zo} respectively, and the azimuthal magnetic field just outside the beam is B_θ. The beam is then described by the following four equations:

Conservation of flux;

$$r_b^2 B_{zi} + (r_w^2 - r_b^2) B_{zo} = 0 \ , \tag{3}$$

Radial pressure balance;

$$\frac{N\gamma m_o v_\theta^2}{2\pi\, r_b^2} + \frac{B_{zi}^2}{8\pi} = \frac{B_{zo}^2}{8\pi} + \frac{B_\theta^2}{8\pi} \tag{4}$$

Ampere's Law;

$$\frac{B_{zi} - B_{zo}}{4\pi} = \frac{Nev_\theta}{2\pi r_b c} \ , \tag{5}$$

and conservation of canonical angular momentum;

$$\frac{e}{2c} r_b^2 B_{zi} + \gamma m_o r_b v_\theta = \frac{e}{2c} r_c^2 B_c \ , \tag{6}$$

where r_c and B_c are the radius of the cathode and the magnetic field at the cathode, respectively. The above equations are used to derive:

$$\frac{B_{zo}}{B_{\theta w}} = \left(\frac{\tan^2\alpha(1 + \gamma/\nu) - 1}{2} \right)^{\frac{1}{2}} \tag{7}$$

$$\frac{r_b^2}{r_w^2} = \frac{1}{2} (1 - \cot^2\alpha + \gamma/\nu) \tag{8}$$

and

$$r_b^2 B_{zi} = r_c^2 B_c \left(\frac{1 + \cot^2\alpha - \gamma/\nu}{1 + \cot^2\alpha + \gamma/\nu} \right) \tag{9}$$

where $\nu = \frac{Ne^2}{m_o c^2}$ is the Budker parameter (the number of beam electrons per unit length times the classical electron radius) and $B_{\theta w} = \frac{r_b B_\theta}{r_w}$ is the azimuthal field at the tube wall. Eq. (9) can be rewritten by dividing through by $B_{\theta w} = 2I/r_w c$ and using Eqs. (7) and (8) to get

$$\frac{cr_c^2 B_c}{2Ir_w} = \left(\frac{\tan^2\alpha\ (\gamma/\nu + 1) - 1}{2}\right)^{1/2} \left(\frac{1 + \cot^2\alpha + \gamma/\nu}{2}\right). \qquad (10)$$

Eliminating α from Equations (7) and (10), $\frac{B_{zo}}{B_{\theta w}}$ can be plotted as a function of $\frac{cr_c^2 B_c}{2Ir_w}$. This is shown in Fig. 2 with ν/γ as the parameter. Values of α are shown on the right hand scale corresponding to $\nu/\gamma = \infty$. Results from the experiment are also shown: here the pitch angle was changed by varying either B_c (circles) or I (triangles) and the corresponding values of $B_{zo}/B_{\theta w}$ measured. I was varied by changing the diode current and determined by measuring $B_{\theta w}$. These measurements were taken at a hydrogen fill pressure of 150 mTorr, at which the beam current was equal to the diode current within the accuracy of measurement (no current neutralization). The experimental points in Fig. 2 fall close to the $\nu/\gamma = \infty$ curve, rather than the $\nu/\gamma = 2$ curve, which is the value the beam would have if propagating freely. This suggests that the density of the rotating beam is enhanced over the density in the diode, and the enhancement is larger than the factor of sec α that would be estimated simply from the rotation.

The density of the beam can also be derived from Eq. (1) if v_b is known. As is shown in Section IV, typically, $v_b \approx .06$ c at 150 mTorr. Thus $N \approx 2.7 \times 10^{14} cm^{-1}$, and $\nu/\gamma_o \approx 25$. Also, as derived in the Appendix,

$\gamma_{beam} < \gamma_o$, thus further enhancing ν/γ. It thus appears that the rotating beams in this experiment are sufficiently dense that the γ/ν terms in Eqs. (7) through (10) may be neglected. This is equivalent to neglecting the centrifugal force on the electrons, so that in the absence of transverse pressure gradients, the beam currents will take up a force-free configuration. This was pointed out previously by Yoshikawa, who considered the case of a solid cylindrical beam.[14] In the dense beam limit, the pitch angle of the beam is a function of $cr_c^2 B_c/2Ir_w$ only (see Eq. (10) with $\gamma/\nu = 0$). This is plotted in Fig. 3.

In the large ν/γ limit, several conclusions can be drawn. From Eq. (8) equilibrium is possible only if $\alpha > 45^0$; furthermore, the equilibrium radius of the beam is the same as that of a force-free plasma carrying identical currents, and, as shown previously,[13] the radius and magnetic fields of the plasma currents which persist after the beam has left satisfy Eq. (7) and Eq. (8) with $\gamma/\nu = 0$. From Eq. (9), the axial flux inside the beam is equal to that inside the cathode to an accuracy of order (γ/ν). This means that the field lines are drawn out of the diode and the half-cusp is carried down the tube at the head of the beam. The small difference in fluxes gives the electrons, through Eq. (6), their azimuthal velocity v_θ, which because of this small difference is only a small fraction of c (typically, $v_\theta \sim 3 \times 10^9 cm.sec^{-1}$ in this experiment). However, as v_θ decreases, N increases, and the product Nv_θ in Eq. (5) is maintained so as to give the flux-conserving axial field in the beam.

For dense beams such as these, the single-particle picture[15] of the action of the cusp on the beam is not appropriate. In particular, the prediction of a critical field B_{crit} above which a particle cannot propagate

through the cusp is no longer valid, For a half cusp, B_{crit} should have twice the value for a full cusp, and be given by

$$B_{crit} = 2\beta\gamma m_o c^2/er_c \qquad (11)$$

where m_o, β and γ have their usual relativistic meanings. For the conditions of this experiment, $B_{crit} \cong 2700$ gauss, but full propagation was observed up to $B_c \cong 7000$ gauss (extreme right-hand circle in Fig. 2), the limit of the cusp field coil.

IV. Propagation of the rotating beam

The measured velocity of propagation, as a function of hydrogen fill pressure, is shown in Fig. 4. The velocity was determined from the difference in the time of arrival of the B_θ field at two magnetic probes spaced 15 cm and 65 cm from the diode. Experiments with different separation between the probes confirmed that the velocity was sensibly constant along the tube. The velocity falls sharply with pressure below 70 mTorr: the beam current is reduced, both the magnitude and persistance time of the induced currents decrease, and no propagation is observed at 40 cm from the cusp. In this regime insufficient plasma is produced on a fast enough time scale to achieve charge neutralization,[16] and the beam expands rapidly to the wall under its own electrostatic forces.

At pressures above 150 mTorr the axial current is uniform along the length of the tube; the beam is charge-neutralized, and electrostatic effects are unimportant. However, the beam front velocity is still only a small fraction of the velocity of light. Because the radial field of the half-cusp is carried down the tube at the front of the beam, and $v_\theta << c$, a newly injected electron will travel axially along the beam

until it reaches the beam front, where it will be reflected and, in the process, lose a small fraction of its energy. (The change in the energy of a charged particle reflected from a moving magnetic field is derived and discussed in the Appendix.) Returning to the diode, the electron passes through the anode foil, is reflected by the applied electric field in the diode, and thus re-injected into the beam. Therefore, the beam consists of an enhanced density of reflexing electrons having a distribution of axial energies with a mean energy $eV < eV_o$, where V_o is the diode potential, and a mean drift velocity $v_b = I/Ne$. This process is illustrated in Fig. 5.

In the steady state, v_b is determined by the balance between the power being injected from the diode and the power required to establish new beam and magnetic field. Thus

$$IV_o = (\tfrac{1}{2} L f^2 I^2 + NeV) v_b \ , \tag{12}$$

where L is the inductance per unit length of the beam, and the factor f ($0 < f < 1$) has been introduced to allow for the possibility that a fraction ($1 - f$) of the injected beam current may be neutralized by some plasma return current. In the limit of a large v/γ, completely unneutralized beam, L is a function only of the pitch angle and may be derived from

$$\tfrac{1}{2} L I^2 = \int_0^{r_w} \frac{(B_z^2 + B_\theta^2)}{8\pi} 2\pi r dr \ . \tag{13}$$

By expressing both the magnetic field components in terms of the axial current, it can be shown that

$$L = \frac{1}{c^2} \left(\left(1 - \frac{r_b^2}{r_w^2}\right) \tan^2 \alpha + 2 \log \frac{r_w}{r_b} \right), \tag{14}$$

where r_b/r_w is obtained from Eq. (8). L is plotted as a function of α in Fig. 6.

The energy required to produce new magnetic field comes from the work done by the beam particles as they advance the beam front. Since $v_b \ll c$, the beam can be treated as a gas doing work on a piston. The pressure of the beam is given by

$$p = (g-1)\frac{NeV}{A}, \tag{15}$$

where g is the effective ratio of specific heats and A is the cross-sectional area of the beam. Then

$$\tfrac{1}{2}Lf^2I^2v_b = pAv_b = (g-1)NeVv_b, \tag{16}$$

and so from Eqs. (12) and (16), converting to practical units

$$\frac{v_b}{c} = \frac{2(g-1)}{g}\frac{Z}{30f^2L}, \tag{17}$$

where Z is the impedance of the injected beam in ohms and L is in nanohenries.cm^{-1}.

For a one-dimensional electron gas, g = 3 if the electrons are non-relativistic, and goes to g = 2 in the ultrarelativistic limit. The value to be used in intermediate cases is found in the Appendix, where the distribution of electron velocities is derived. The fraction of the injected electron energy that is converted into magnetic energy is (g-1)/g, and lies in the range 67% - 50%.

The role of the self-magnetic field energy in determining the propagation velocity of a beam through the power balance was pointed out

previously by Ecker and Putnam,[17] who performed a similar analysis for a non-rotating beam, but with the assumption that the beam electrons passed radially out of the beam front to the wall. There was therefore no enhancement of the beam density, which is equivalent to neglecting the second term on the r.h.s. of Eq. (12), and the predicted beam front velocity was given by

$$\frac{v_b}{c} = \frac{0.07Z}{L} \qquad (Z \text{ in ohms, } L \text{ in nH}\cdot\text{cm}^{-1}) \tag{18}$$

which is about twice the value given by the present model. In their experiments with straight, and presumably pinched, beams, Ecker and Putnam were not able to determine L with sufficient accuracy to verify Eq. (18) quantitatively, although an increase in v_b with Z was observed.

The inductance of a dense rotating beam has a broad minimum of 2.9 nH.cm^{-1} at $\alpha = 55^0$ (Fig. 6). In the present experiments, $V_o \tilde{=} 900$ kV ($\gamma_o = 2.6$) and the corresponding value of g is 2.5 (see Appendix). Thus Eq. (17) becomes

$$\frac{v_b}{c} = \frac{0.04Z}{f^2 L} . \tag{19}$$

The straight line in Fig. 7 represents v_b/c as a function of Z from Eq. (19) with f = 1 and L = 3.0 nH.cm^{-1}. The points represent experimental results when, with B_c fixed at 4.2 kG, Z was varied by changing the anode-cathode gap in the diode. While this changed the current, and hence the pitch angle, these data were taken in the range where the pitch angle was measured to be $50^0 < \alpha < 60^0$ over which L does not vary significantly.

The pressure was 150 mTorr, at which $f \stackrel{\sim}{=} 1$.

As the pressure is increased above 150 mTorr, induced plasma return currents reduce the net beam current to below the injected beam current. From a comparison of the net and injected currents, f is found to fall to about 0.8 at 400 mTorr. At this pressure v_b is observed (Fig. 4) to increase by 56% over its value at 150 mTorr, in close agreement with the prediction of Eq. (19). The increase in velocity with pressure is therefore consistent with the increase in the degree of current neutralization.

With the diode impedance held constant at Z = 7 ohms, the pitch angle was varied by varying B_c. The points in Fig. 8 show the observed v_b plotted against measured values of $B_{zo}/B_{\theta w}$. The solid line shows the prediction of the model, using Eq. (19) with L derived from Eqs. (7), (8) and (14), and with f = 0.8, appropriate for the pressure of 400 mTorr at which the results were taken. The results of Figs. (4), (7) and (8) all show excellent agreement with the predictions of the model.

V. Further experiments

Although all the results described so far are consistent with the theoretical model, it is desirable to have more direct evidence to support the claim that the beam is in fact made up of reflexing electrons. To this end two further experiments were carried out.

In the model the distinction is made between the pitch angle of the current $\alpha = \tan^{-1}(v_\theta/v_b)$, and the pitch angle of the beam electrons $\theta = \sin^{-1}(v_\theta/\beta_o c)$, where $\beta_o c$ is the injection velocity. To measure the pitch angle of the electrons, 6 mm dia. lucite rods were placed across a diameter of the tube, and, following the method of Roberson et al.[18] it was possible to deduce the direction from which electrons struck the rod

by measuring the resulting damage pattern. When α, derived from magnetic field measurements, was $\sim 60^0$, it was found that $\theta \sim 5^0 \pm 5^0$. This is consistent with $v_b \sim 0.1$ c, and a density enhancement of the rotating beam of about a factor of ten.

For the second experiment, a 1 mm dia. tungsten wire was placed across a diameter of tube, 25 cm from the half-cusp, and the X-rays from the wire were detected by a collimated scintillator-photomultiplier with a response time of $\lesssim 5$ ns. Signals from the X-ray detector are shown in the upper traces of Fig. 9; the lower traces show the current in the diode. The X-ray signal at first roughly follows the current, but starts to fall at a time which corresponds to the time of arrival of the beam front at the conducting screen which defines the end of the tube. As can be seen, the fall in the X-ray signal occurs later when the end screen is moved further from the diode, and in both cases the width of the X-ray pulse is less than that of the diode current. This result is interpreted as a reduction in the density of beam electrons when the front reaches the end wall and the reflection process ceases; the axial current is then carried by beam electrons which make only one pass down the tube with their full injected velocity, and the beam density falls to a fraction $v_b/\beta_o c$ of its former value. Since v_θ is not changed, the azimuthal current that maintains the axial magnetic field is now carried mainly by plasma electrons.

No attempt has been made to interpret the X-ray signals quantitatively: since the reflexing electrons have a large velocity spread (see Appendix) this would be a very difficult task. However, some comment can be made on the decay of the X-ray signal. If electron reflection ceased at the instant the beam arrived at the end screen, the density decay time would be

about the transit time of a beam electron, which is a few nanoseconds. The decay of the X-ray signal is 15-25 ns, suggesting that the reflection process does not terminate abruptly. This can be understood by considering the approach of the rotating beam to the conducting end screen: the radial magnetic field at the head of the beam (Fig. 5) cannot penetrate the conductor and becomes compressed, acting as a barrier to the passage of the beam electrons. Electric fields will be induced that maintain the current with plasma electrons, and a rather complicated situation arises that delays the complete "opening" of the magnetic field. Thus the beam electrons cannot enter the end screen instantaneously. A similar situation arises when a thin (25 μ) titanium foil is placed in the path of the beam: experiments show a rotating beam will not propagate through the foil, whereas a non-rotating beam penetrates without difficulty. The difference is attributed primarily to the radial magnetic field at the head of the rotating beam.

VI. Conclusions

This paper has described a theoretical and experimental study of a charge-neutralized, hollow, rotating relativistic electron beam propagating down a metal tube in the absence of an external guide field. A model has been developed in which the radial equilibrium of the beam is derived from the conservation of flux, particles, and canonical angular momentum, and the velocity of propagation of the beam is derived from considerations of power balance. In the range of interest, the beam is found to propagate quite slowly ($v_b \sim 0.05 - 0.1\ c$) and have an enhanced density over that of a freely propagating beam. This density enhancement arises from multiple reflections of the electrons between the beam front and the diode, and can

be sufficient to make $\nu/\gamma >> 1$. In this case the currents of the beam take up a force-free configuration, and the axial magnetic flux inside the beam is almost the same as that initially in the cathode. This leads to a picture of the propagating beam stretching the magnetic lines of force from the cathode, the velocity of propagation being determined by a balance between the power injected from the diode and the power required to create new beam and the associated stretched magnetic field. This model is found to give good qualitative and quantitative agreement with experimental results.

Although the model is derived in the limit of a very thin annular beam, photographs of the plasma created by the beam show $\delta/r_b \sim 0.2$ and the beam itself may be somewhat thinner, so the application of thin-beam model to interpret the experimental results is justified.

The model is useful when considering the applications of rotating electron beams. One application is the creation of magnetically confined plasmas inside closed metal systems, such as imploding liners;[19] another application is the collective acceleration of ions trapped in the potential well of the negative space charge which exists at the head of the beam.[20] In the latter application, the ability to control the beam front velocity by changing the pitch angle of the beam current may prove especially useful.

Acknowledgements

The authors are indebted to Dr. C.A. Kapetanakos, Dr. C.W. Roberson, Dr. R.A. Meger, Dr. D. Nagel and Dr. F.C. Young for their helpful suggestions, and acknowledge the technical assistance of Mr. A.K. Kinkead.

This work was supported by the Office of Naval Research and the U.S. Department of Energy.

REFERENCES

1. K.R. Chu and N. Rostoker, Phys. Fluids 17, 813 (1974).
2. K.R. Chu, C.A. Kapetanakos and R.W. Clark, Appl. Phys. Lett. 27, 185 (1975).
3. C.A. Kapetanakos, W.M. Black and K.R. Chu, Phys. Rev. Lett. 34, 1156 (1975).
4. C.A. Kapetanakos, W.M. Black, and C.D. Striffler, Appl. Phys. Lett. 26, 368 (1975).
5. D.A. Hammer, A.E. Robson, K.A. Gerber and J.D. Sethian, Phys. Lett. 60A, 31 (1977).
6. K. Molvig and N. Rostoker, Phys. Fluids 20, 494 (1977).
7. C.W. Roberson, D. Tzach and N. Rostoker, Appl. Phys. Lett. 32, 214 (1978).
8. J.D. Sethian, D.A. Hammer, K.A. Gerber, D.N. Spector, A.E. Robson and G.C. Goldenabum, Phys. Fluids 21, 1227 (1978).
9. C.W. Roberson, Nucl. Fusion 18, 1693 (1978).
10. M. Friedman, Phys. Rev. Lett. 24, 1098 (1970).
11. R.E. Kribel, K. Skinsky, D.A. Phelps and H.H. Fleischmann, Plasma Physics 16, 113 (1974).
12. H.L. Berk and D. Pearlstein, Phys. Fluids 19, 1831 (1976).
13. J.D. Sethian, K.A. Gerber, D.N. Spector, and A.E. Robson, Phys. Rev. Lett. 41, 798 (1978).
14. S. Yoshikawa, Phys. Rev. Lett. 26, 295 (1971).
15. G. Schmidt, Phys. Fluids 5, 994 (1962).
16. N. Rostoker, Proceedings VIIth International Conference on High Energy Accelerators., Yerevan, USSR, p. 509 (1969).

17. B. Ecker and S. Putnam, IEEE Transactions on Nuclear Science, Vol. NS-24, No. 3, p. 1665 (1977).

18. C.W. Roberson, G. Saenz, and D. Tzach, Rev. Sci. Instrum. 48, 804 (1977).

19. J.D. Sethian and A.E. Robson, J. Mag. and Mag. Materials 11, 416 (1979).

20. J.D. Sethian, R.A. Meger, R.A. Mahaffey, and D.N. Spector, Proceedings IEEE International Conference on Accelerator Technology, San Francisco, CA, 1979.

21. E. Fermi, Phys. Rev. 75, 1169 (1949).

Appendix

The velocity distribution of the electrons in the beam will be derived by tracing the path of electrons on a z - t diagram (Fig. 10) as they make successive reflections from the beam front and the diode. All motion is assumed to be in the axial (z) direction, which is justified as long as $v_z >> v_\theta$. The beam front moves with constant velocity $v_b = \hat{\beta}c$, and its path is represented in Fig. 10 by the line F, which makes an angle $\phi = \tan^{-1}\hat{\beta}$ with the time axis. Injection of a constant-current beam begins at t = 0. Each electron is injected with velocity $\beta_0 c$, and after 1, 2 ... n reflections from the moving front has velocity $\beta_1 c$, $\beta_2 c$ ... $\beta_n c$ respectively. Each collision with the beam front results in a reduction in the velocity of the electron; each reflection from the diode is assumed to change the sign but not the magnitude of the electron velocity.

The path of an electron that makes its $(n+1)^{th}$ collison with the beam front at time t = T is represented by the line P. The time t_n at which this electron made its n^{th} collision can be derived geometrically from Fig. 10. Thus:

$$\frac{T \tan \phi}{\sin \theta_n \sin(\theta_n + \phi)} = \frac{T - t_n}{\cos \phi \sin 2\theta_n} \qquad \text{(A 1)}$$

where $\theta_n = \tan^{-1}\beta_n$. From this we derive

$$\frac{t_n}{T} = \frac{\tan \theta_n - \tan \phi}{\tan \theta_n + \tan \phi} = \frac{\beta_n - \hat{\beta}}{\beta_n + \hat{\beta}} \quad . \qquad \text{(A 2)}$$

Repeating this process we obtain

$$\frac{t_{n-1}}{T} = \frac{(\beta_n - \hat{\beta})}{(\beta_n + \hat{\beta})} \cdot \frac{(\beta_{n-1} - \hat{\beta})}{(\beta_{n-1} + \hat{\beta})} \qquad \text{(A 3)}$$

where t_{n-1} is the time of the $(n-1)^{th}$ collision with the front. The time τ_n at which this electron was injected is thus given by

$$\tau_n = T \cdot B_n \cdot B_{n-1} \ \ldots\ldots \ B_1 \cdot B_0 \qquad \text{(A 4)}$$

where $B_i = \frac{\beta_i - \hat{\beta}}{\beta_i + \hat{\beta}}$ $(i = 1, n)$ and $B_0 = 1 - \frac{\hat{\beta}}{\beta_0}$.

The change in velocity of an electron colliding with the slower-moving beam front arises in the same manner as in the theory of acceleration of cosmic rays by moving magnetic fields,[21] except that in the present case the electron is always overtaking the front and so loses energy at each encounter. The electrons are actually turned around by the radial magnetic field at the head of the beam (Fig. 5) and lose energy in the induced azimuthal electric field. At low pressures the axial electrostatic field of the unneutralized space charge will assist the reflection process, but in all cases the effect of the collision on the electron can be obtained by a simple application of special relativity without reference to the detailed mechanism of the collision. The initial energy and momentum is first transformed into the frame of the moving front: in this frame the collision is elastic, the momentum changes direction and the energy is unchanged. Transforming back to the laboratory frame we obtain the values of energy and momentum after the collision. It is found[21] that

$$\beta_i = \frac{\beta_{i-1}(1+\hat{\beta}^2) - 2\hat{\beta}}{1 - 2\hat{\beta}\beta_{i-1} + \hat{\beta}^2} \qquad \text{(A 5)}$$

and

$$\frac{\gamma_i}{\gamma_{i-1}} = \frac{1 - 2\hat{\beta}\beta_{i-1} + \hat{\beta}^2}{1 - \beta^2} \qquad \text{(A 6)}$$

where the subscripts i - 1, i refer respectively to the electron before and after the i^{th} collision. Given β_0 and $\hat{\beta}$ we may obtain β_1, β_2 .... β_n by successive applications of (A 5), and then through (A 4) obtain τ_0, τ_1 ..... τ_n.

The total number of electrons in the beam at time T is

$$N_{tot} = \frac{IT}{e} = Nv_bT \qquad \text{(A 7)}$$

where I is the beam current and N the number of electrons per unit length. Of this number, those electrons that have made n collisions were injected between the time τ_n and τ_{n-1} and therefore the fraction of the distribution that has velocity β_n is

$$f_n = \frac{\tau_n - \tau_{n-1}}{T} . \qquad \text{(A 8)}$$

Eventually each electron will make a collision with the front which reduces its velocity to less than the front velocity, and no further collisions will occur. If the last collision is the m^{th}, then

$$f_m = \frac{\tau_m}{T} \quad . \tag{A 9}$$

Given $\hat{\beta}$ and β_o (or γ_o) we can compute the distribution of electron velocities in the beam. Fig. 11 shows the results of a case typical of the experiment, namely $\hat{\beta} = 0.05$, $\gamma_o = 3$. There are 18 collisions with the beam front, and therefore 19 velocity groups. For all practical purposes this may be regarded as a continuum. Note that in this model, where the front is assumed to have constant velocity and the beam current is assumed to rise instantaneously, the distribution is established at t = 0 and maintained indefinitely.

Each group of electrons transfers momentum to the beam front as it is reflected: the n^{th} group exerts a pressure on the front given by

$$P_n = \frac{1}{2} f_n (\beta_n - \hat{\beta}) \cdot (\beta_n \gamma_n + \beta_{n+1} \gamma_{n+1}) n m_o c^2 \tag{A 10}$$

where n is the total electron density in the beam. The factor $\frac{1}{2}$ is omitted for the n = 0 (freshly injected) group, since the electrons in this group are all moving in the same direction.

The kinetic energy per unit volume of the n^{th} group is

$$K_n = f_n (\gamma_n - 1) n m_o c^2 \tag{A 11}$$

and so g, the ratio of specific heats of the electrons 'gas' is given by

$$g = 1 + \frac{\sum_{o}^{m-1} P_n}{\sum_{o}^{m} K_n} \qquad \text{(A 12)}$$

and the ratio of the mean kinetic energy of the electrons $\bar{E}$ to their injection energy E_o is given by

$$\frac{\bar{E}}{E_o} = \frac{\sum_{o}^{m} f_n(\gamma_n - 1)}{\gamma_o - 1} \quad . \qquad \text{(A 13)}$$

Table 1 shows values of m, $\bar{E}/E_o$ and g for 21 cases covering a range of initial conditions (γ_o, $\hat{\beta}$). It can be seen that although m, the number of collisions, is sensitive to $\hat{\beta}$, the other quantities are not. Note that in the limit of $\hat{\beta} \to 0$ and $\gamma_o \to 1$ (nonrelativistic case), $\bar{E}/E_o = 1/3$ and g = 3, while in the limit $\gamma_o \to \infty$ (ultrarelativistic case) $\bar{E}/E_o = 1/2$ and g = 2.

Table 1

	$\hat{\beta} = 0.025$			$\hat{\beta} = 0.05$			$\hat{\beta} = 0.1$		
Y_o	m	$\bar{E}/E_o$	g	m	$\bar{E}/E_o$	g	m	$\bar{E}/E_o$	g
2	26	0.381	2.63	13	0.382	2.61	7	0.390	2.57
3	35	0.406	2.46	18	0.408	2.45	9	0.413	2.42
4	41	0.423	2.37	21	0.424	2.36	10	0.429	2.33
5	46	0.434	2.30	23	0.435	2.30	11	0.440	2.27
6	50	0.442	2.26	25	0.443	2.26	12	0.448	2.23
7	53	0.449	2.23	26	0.450	2.22	13	0.454	2.20
8	55	0.454	2.20	28	0.455	2.20	14	0.459	2.18

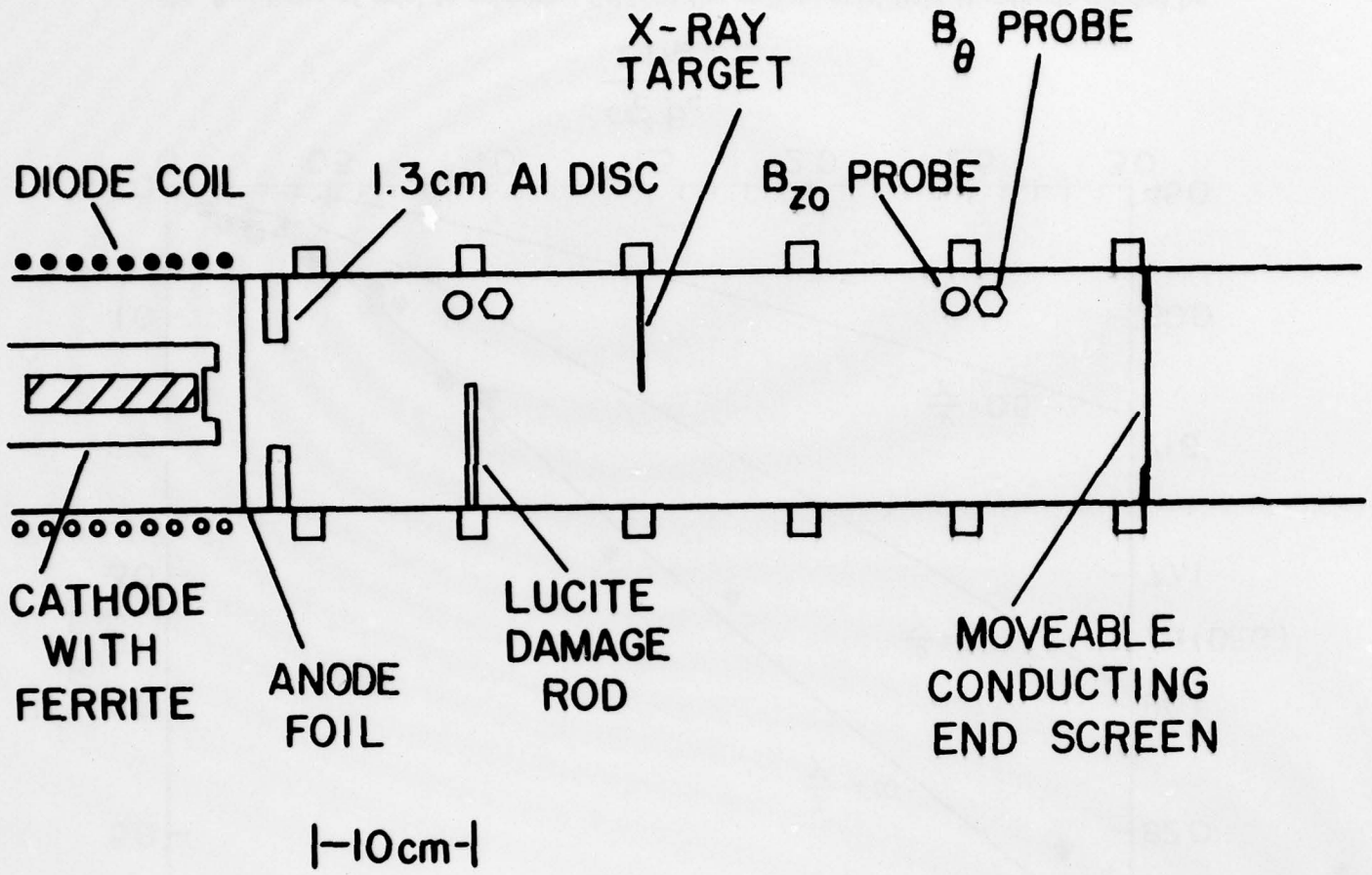

Fig. 1 — The experimental apparatus

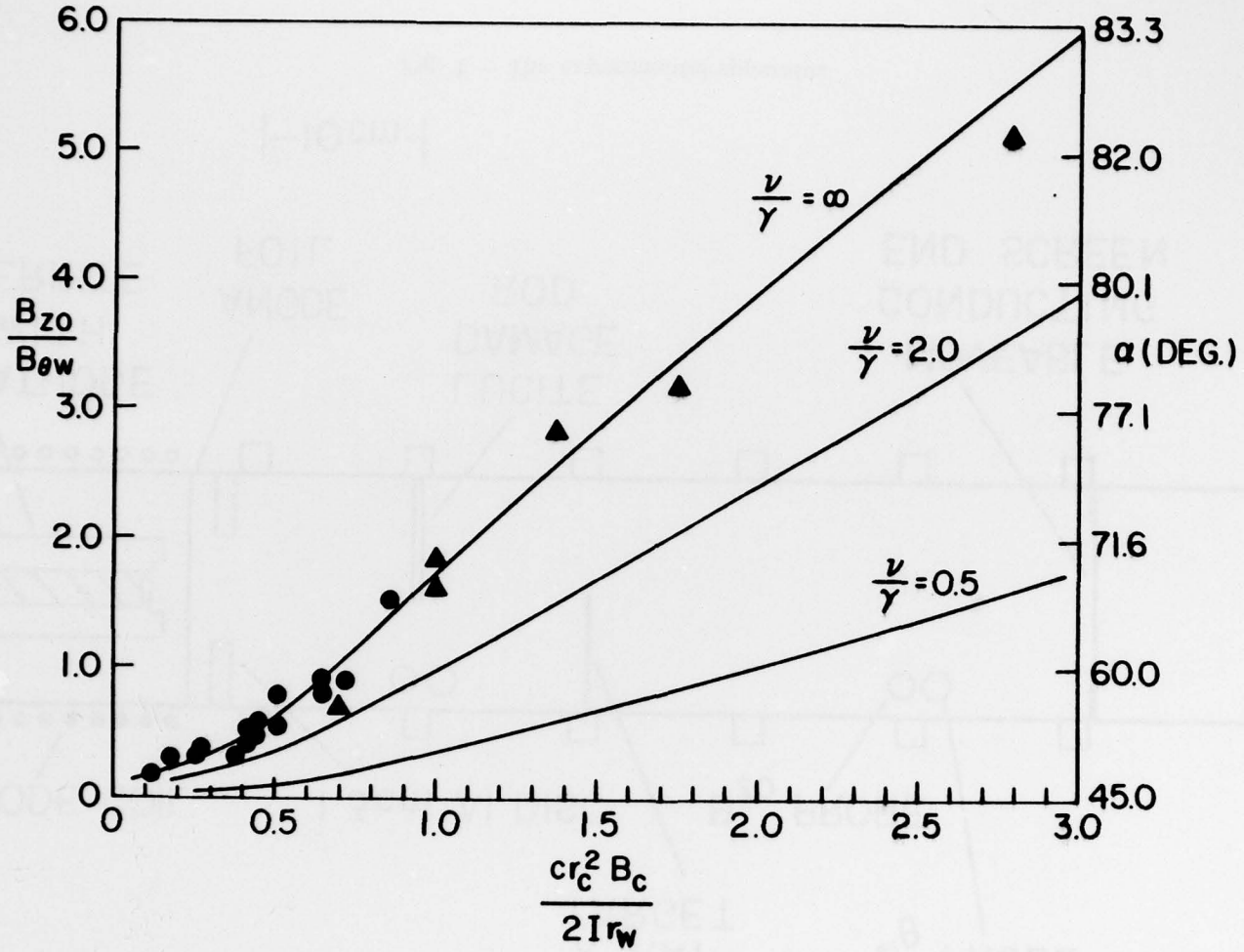

Fig. 2 — Ratio of axial to azimuthal fields at the wall vs. axial field at cathode divided by the beam current, with ν/γ as parameter. The solid lines are the predictions of the model. The angles on the right hand scale correspond to $\nu/\gamma = \infty$. The data points were taken by varying either the cathode field (circles) with the current constant at 70 kA, or beam current (triangles) with the cathode field held fixed at 3.8 kG. The fill pressure was 150 mTorr.

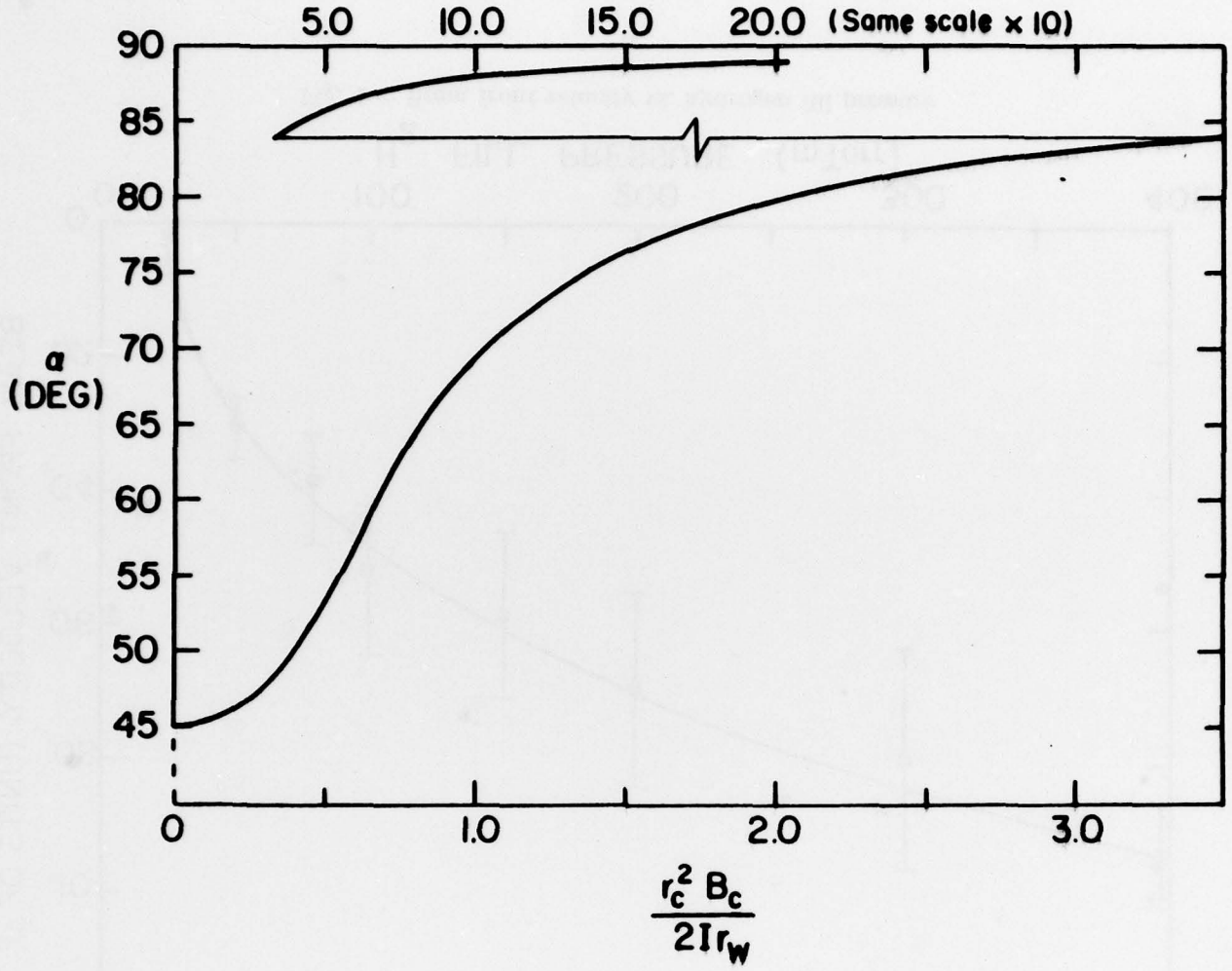

Fig. 3 — Current pitch angle vs. normalized axial flux at the cathode, $\nu/\gamma = \infty$

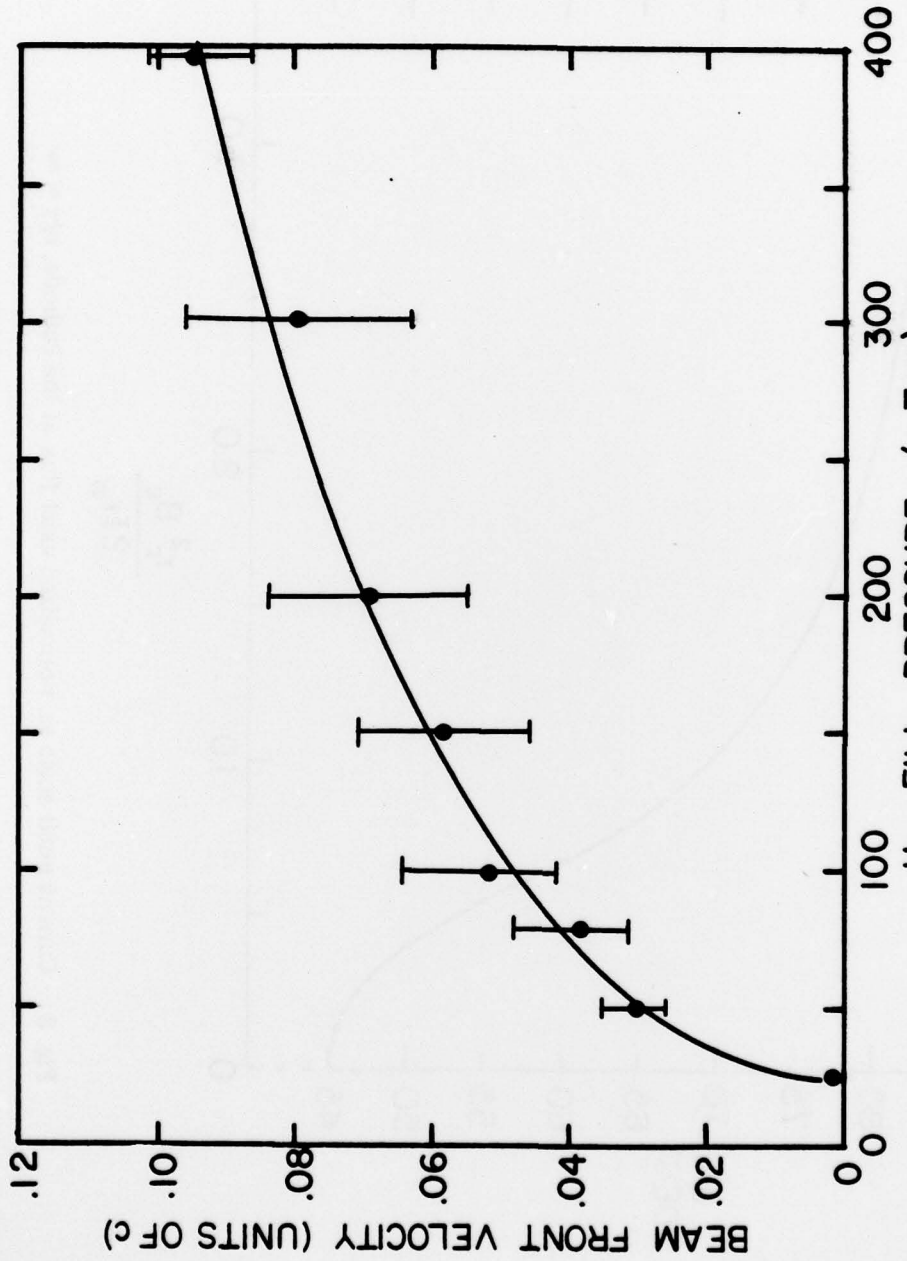

Fig. 4 — Beam front velocity vs. hydrogen fill pressure

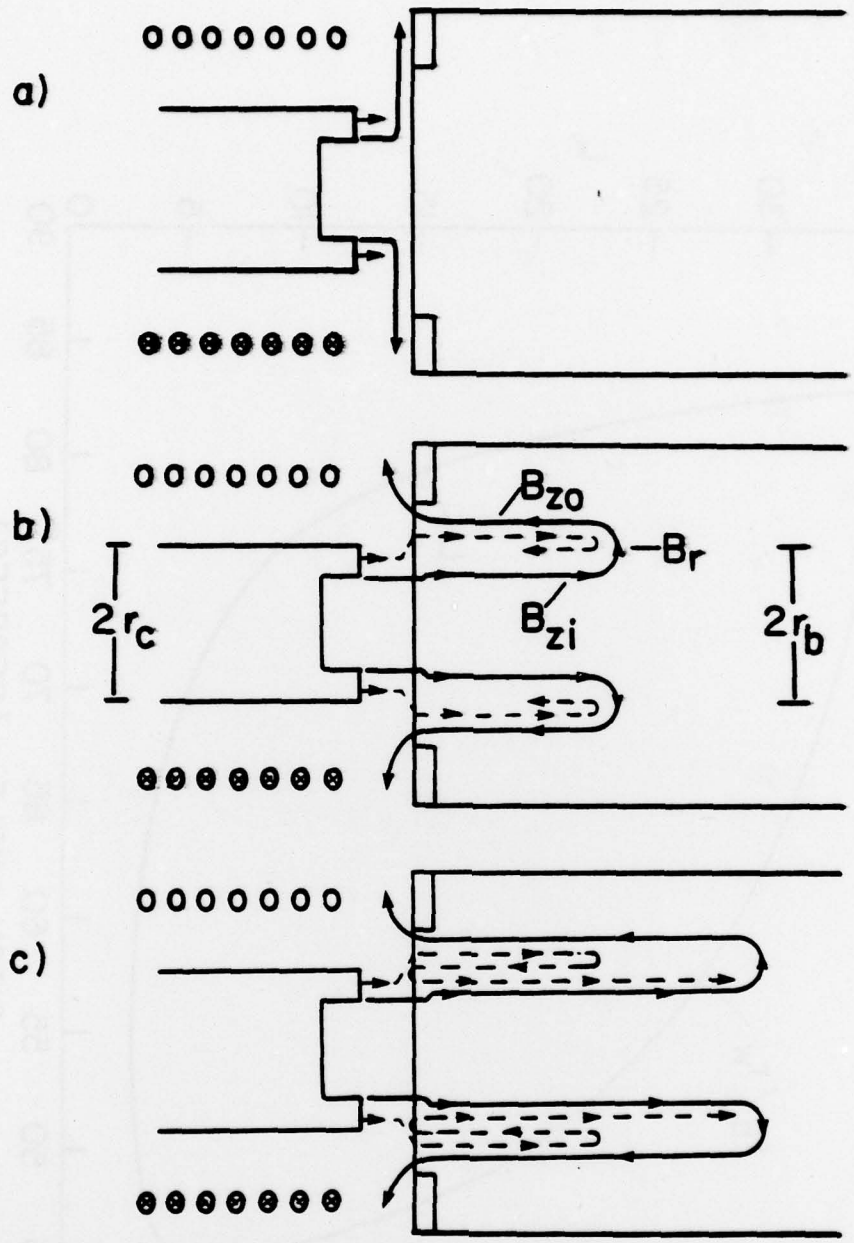

Fig. 5 — Illustration of rotating beam propagation model. Solid lines denote magnetic field lines, broken lines relativistic electron trajectories. For simplicity, the azimuthal components of the magnetic field and electron velocity are not shown. (a) beam is injected into half-cusp field. (b) radial field in cusp causes beam electrons to rotate. The resulting axial field, B_{zi}, closely conserves cathode flux; beam motion is retarded by the need to supply the self-field energy. Fresh beam electrons are reflected from the radial field, B_r, at the front, transferring a small fraction of their energy to the induced field. (c) electrons are reflected in the diode without loss of energy and return to beam front. Reflexing continues until electron velocity is less than beam front velocity.

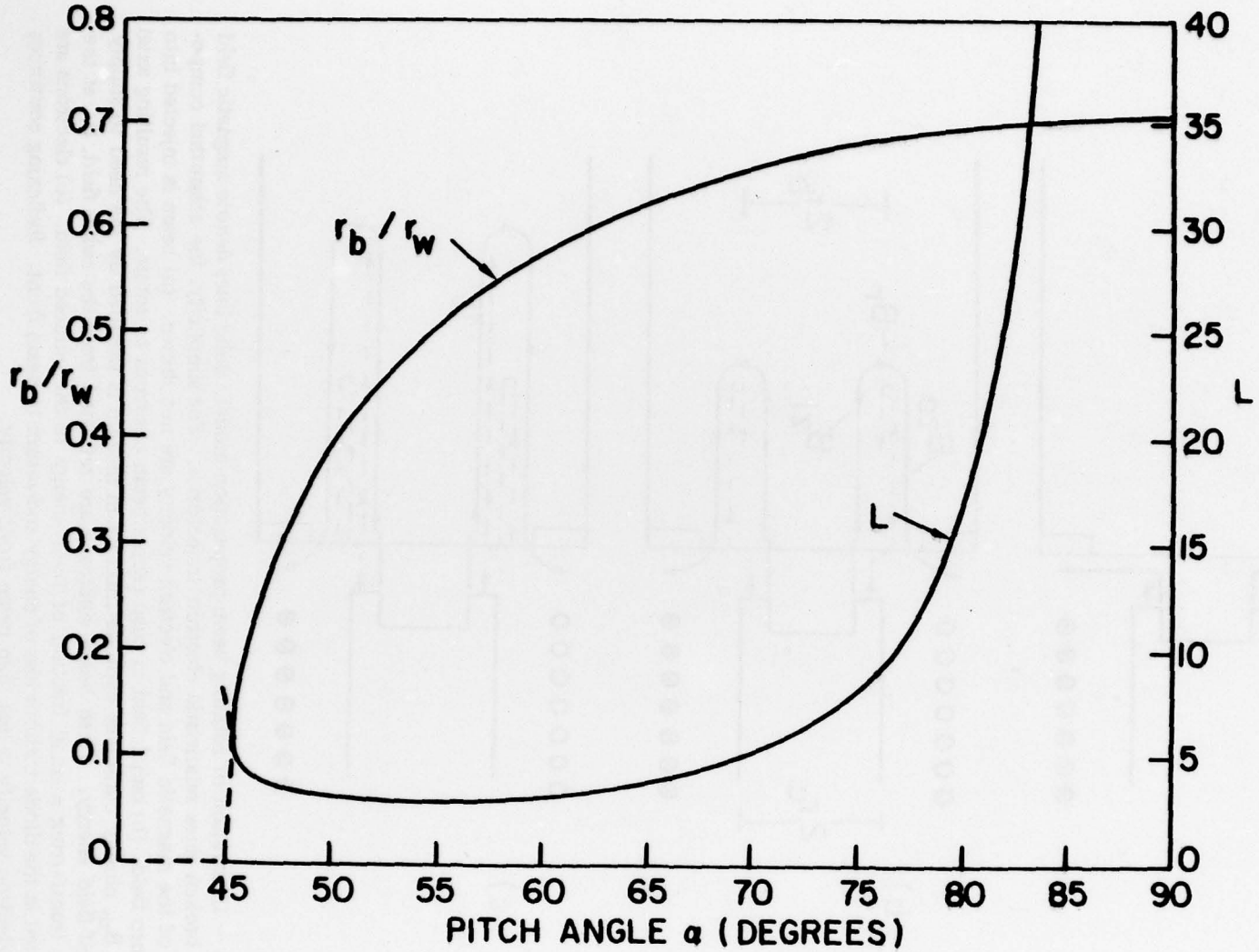

Fig. 6 — Inductance per unit length, in nH.cm^{-1}, as a function of beam pitch angle, with $\nu/\gamma = \infty$

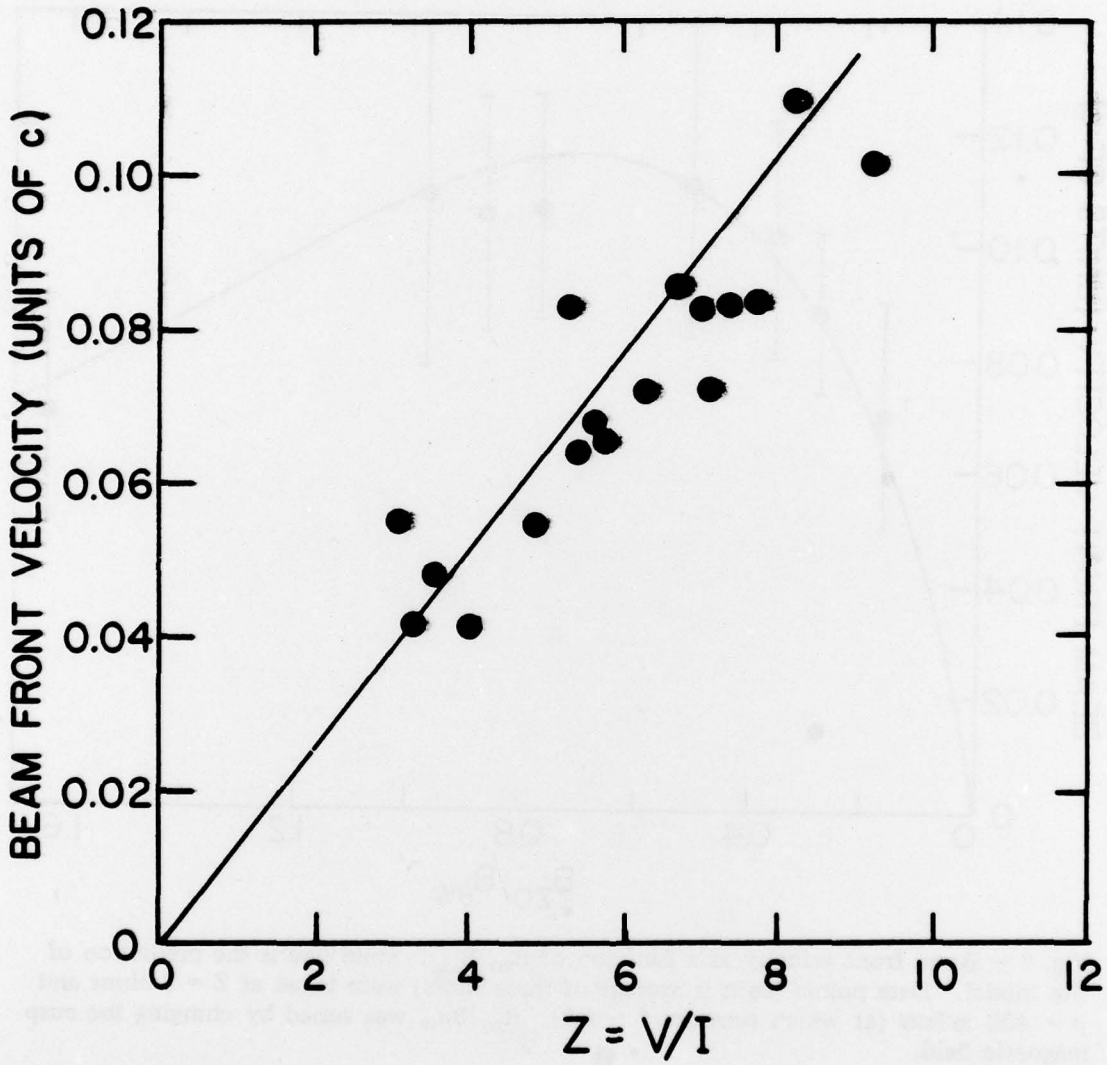

Fig. 7 — Beam front velocity as a function of diode impedance. Solid line is the prediction of the model. L was taken to be 3.0 nH.cm^{-1} from measured ratios of $B_{zo}/B_{\theta w}$ and Fig. 6. Data were taken at p = 150 mTorr, where no current neutralization was observed.

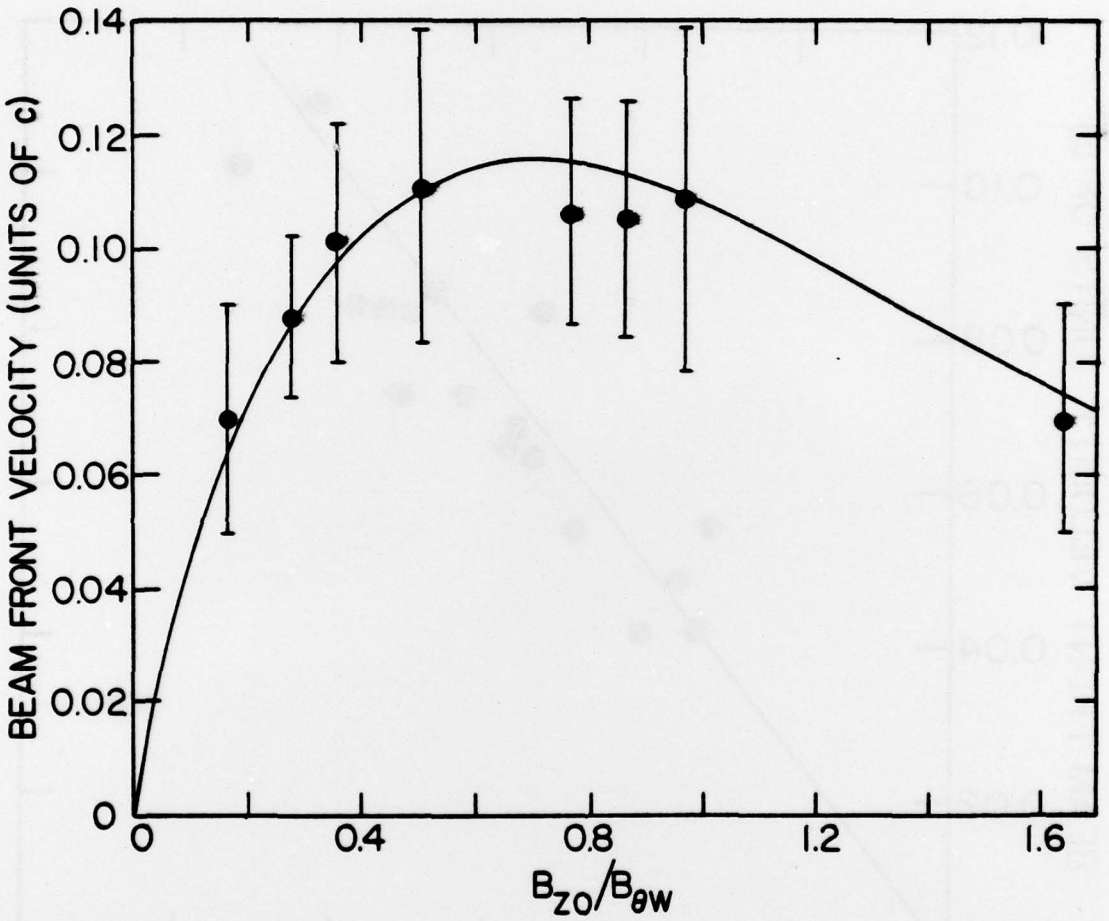

Fig. 8 — Beam front velocity as a function of $B_{zo}/B_{\theta w}$. Solid line is the prediction of the model. Data points (each is average of three shots) were taken at Z = 7 ohms and p = 400 mTorr (at which pressure f ~ 0.8). $B_{zo}/B_{\theta w}$ was varied by changing the cusp magnetic field.

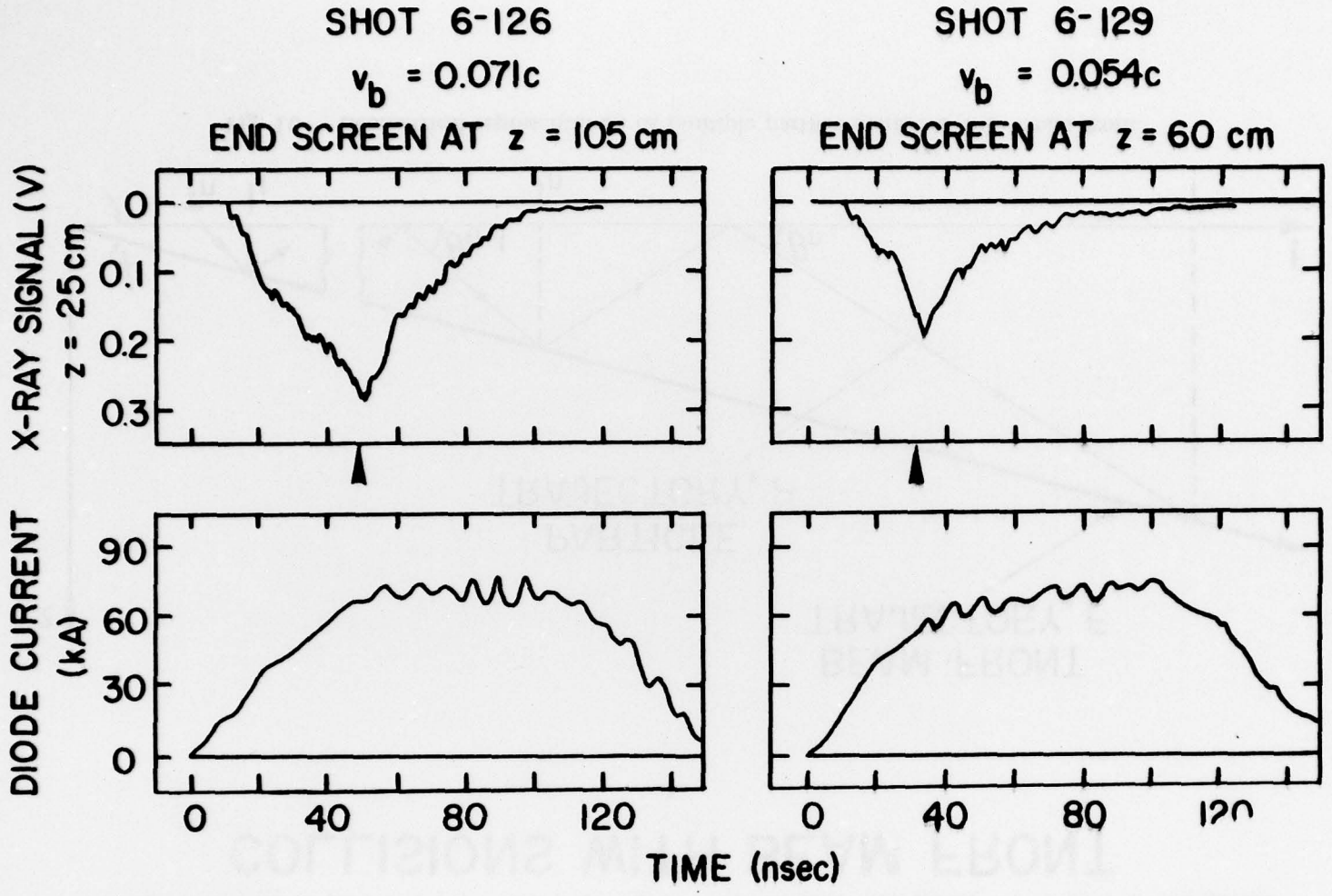

Fig. 9 — X-ray signals (upper) and diode current (lower) for two drift tube lengths. Arrows mark anticipated time of arrival of beam front at the conducting end screen.

REPRESENTATION OF MULTIPLE PARTICLE COLLISIONS WITH BEAM FRONT

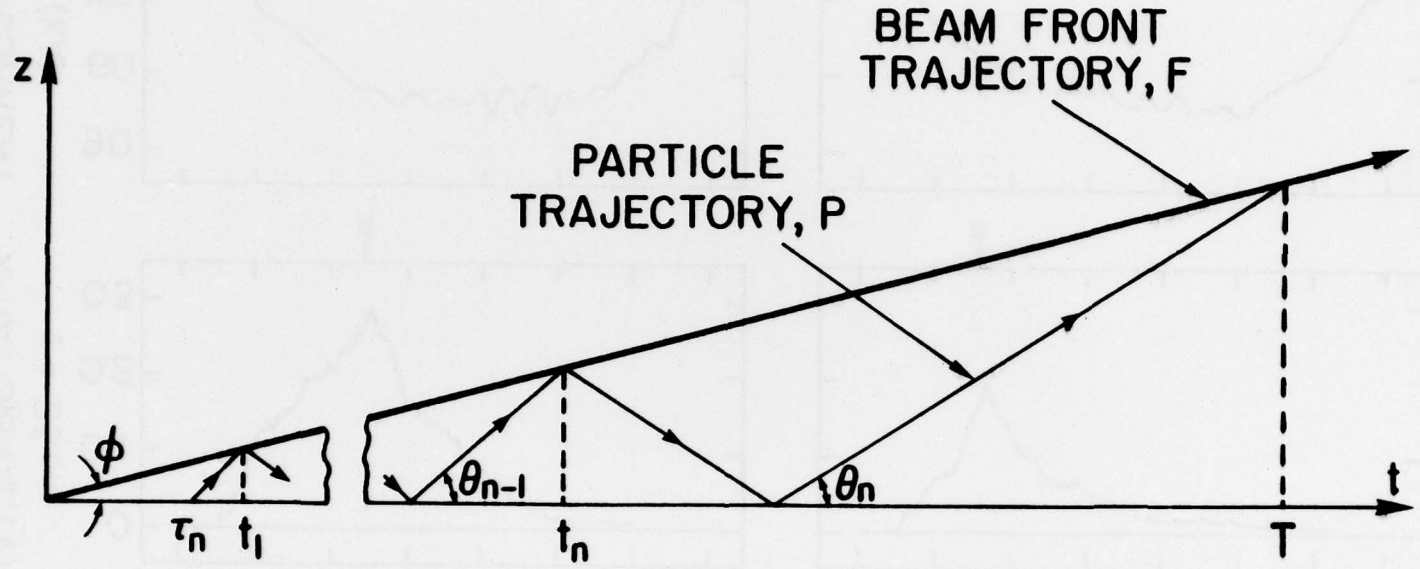

Fig. 10 — Geometrical representation of multiple particle collisions with beam front

DISTRIBUTION OF ELECTRON VELOCITIES IN BEAM

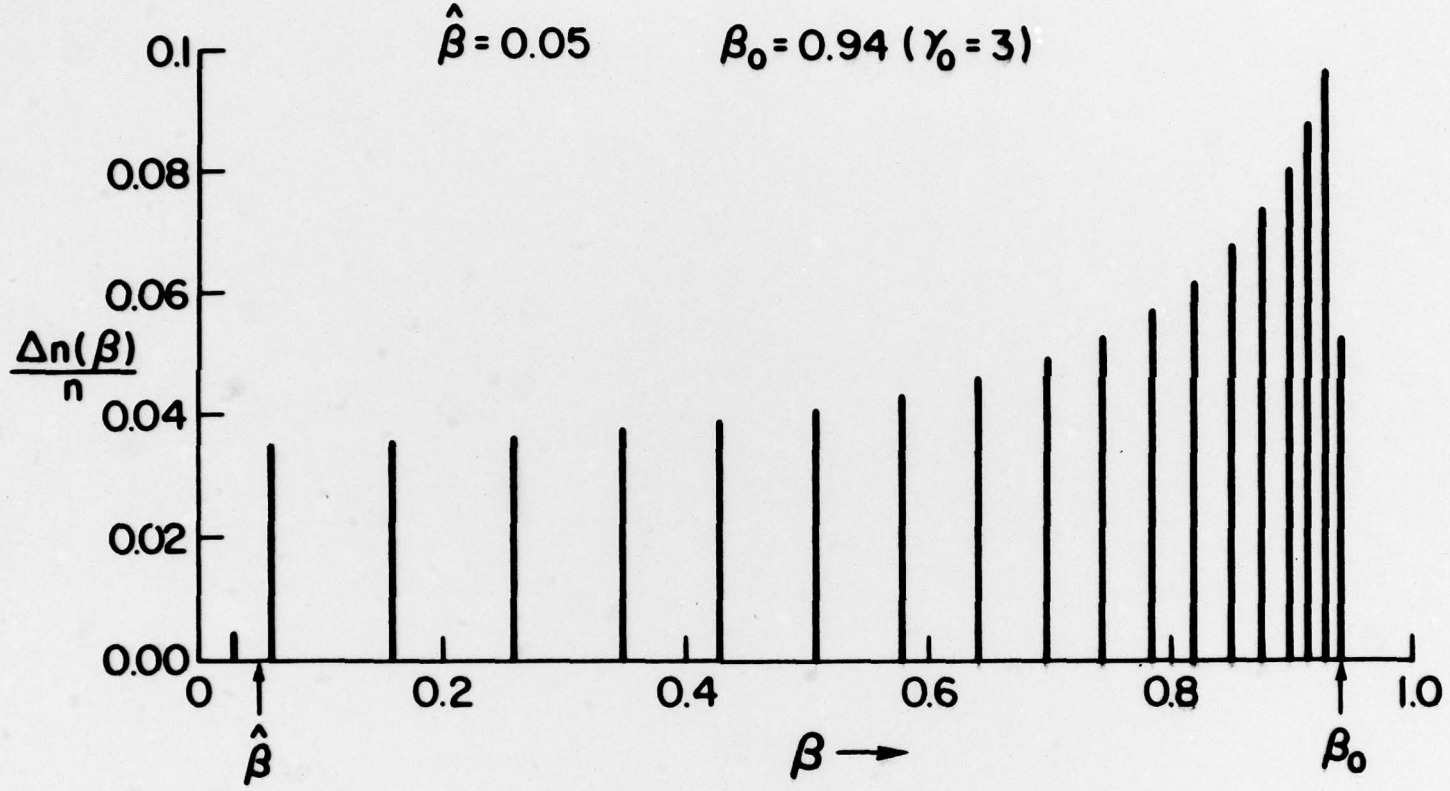

Fig. 11 — Velocity distribution of electrons in the beam